UDK 621.78.019.84:677.494.7
Original scientific article/Izvirni znanstveni članek

ISSN 1580-2949
Mater. Tehnol.

# LONG-TERM DEGRADATION MECHANISMS AND SERVICE LIFE PREDICTION OF BFRP AND GFRP BARS UNDER ALKALINE CORROSION ENVIRONMENTS

## MEHANIZMI DOLGOTRAJNE DEGRADACIJE IN NAPOVED DOBE TRAJANJA Z VLAKNI OJAČANIH POLIMERNIH KOMPOZITOV V ALKALNEM KOROZIJSKEM OKOLJU

**Linjie Chai*, Junkuo Li, Lihuan Wang, Fan Gao, Jia Guo**

Economic and Technological Research Institute, State Grid Hebei Electric Power Co., Ltd., Shijiazhuang 050021, Hebei, China

*Prejem rokopisa – received: 2025-09-16; sprejem za objavo – accepted for publication: 2026-01-09*

doi:10.17222/mit.2025.1566

Fiber reinforced polymer (FRP) composites are increasingly employed in civil infrastructure due to their high strength-to-weight ratio and corrosion resistance, yet their long-term durability in alkaline environments remains a critical concern for structural safety. This study investigated the long-term durability of basalt fiber reinforced polymer (BFRP) and glass fiber reinforced polymer (GFRP) bars that were exposed to alkaline corrosion environments. Accelerated aging tests were conducted at 40 °C and 60 °C to evaluate the degradation in tensile strength, interlaminar shear strength, and moisture absorption. The experimental results demonstrated that both BFRP and GFRP bars exhibited progressive deterioration, with BFRP showing more severe strength loss, particularly at elevated temperatures. Moisture uptake behavior was observed to follow Fickian diffusion in the early stage but later transitioned into nonlinear regimes, indicating structural changes that facilitated accelerated degradation. Scanning electron microscopy revealed that matrix corrosion was dominant at the initial stage, while fiber–matrix debonding and fiber corrosion became predominant with extended exposure, leading to void expansion and corrosion channel formation. An improved Fick-based degradation model was developed to predict the strength retention and service life of FRP bars. The model exhibited good agreement with experimental data, confirming its applicability for life prediction in practical engineering.

Keywords: fiber reinforced polymer, alkaline corrosion, mechanical degradation, service life prediction

Z vlakni ojačani polimerni kompoziti (FRP; angl: Fiber Reinforced Polymer composites) se zaradi visokega razmerja med maso in trdnostjo ter odpornostjo proti koroziji vse pogosteje uporabljajo v civilni infrastrukturi, vendar je pri tem za varnost konstrukcij ključnega pomena njihova dolgotrajna vzdržljivost (angl.: long-term durability) v alkalnih okoljih. V tem članku avtorji opisujejo študijo dobe trajanja oziroma dolgotrajne vzdržljivosti palic iz z bazaltnimi vlakni ojačane polimerne matrice (BFRP; angl.: basalt fiber reinforced polymer) in s steklenimi vlakni ojačane polimerne matrice (GFRP; angl.: glass fiber reinforced polymer), ki so bile izpostavljene alkalnim korozijskim okoljem. Preizkuse pospešenega staranja so izvedli pri 40 °C in 60 °C in ocenjevali padec natezne trdnosti, medplastne strižne trdnosti in absorpcijo vlage. Eksperimentalni rezultati so pokazali, da palice iz BFRP in GFRP postopno propadajo, pri čemer je BFRP kompozit hitreje izgubljal svojo trdnost, zlasti pri povišanih temperaturah. V zgodnji fazi opazovanja so avtorji ugotovili, da absorpcija vlage sledi Fickovi difuziji. Kasneje pa je le-ta prešla v nelinearne režime, kar kaže na strukturne spremembe, ki so pospešile degradacijo. Vrstična elektronska mikroskopija (SEM) je pokazala, da je bila v začetni fazi prevladujoča korozija matrice, medtem ko sta z daljšo izpostavljenostjo prevladovala odcepitev vlaken od matrice in korozija vlaken, kar je vodilo do širjenja praznin in nastanka korozijskih kanalov. Za napovedovanje ohranitve trdnosti in življenjske dobe FRP palic so avtorji tega članka razvili izboljšan Fickov model degradacije. Model se dobro ujema z eksperimentalnimi podatki, kar potrjuje njegovo uporabnost za napovedovanje življenjske dobe v praktičnem inženirstvu.

Ključne besede: z vlakni ojačani polimerni kompoziti, korozija v alkalnem okolju, mehanske poškodbe, napoved dobe trajanja

## 1 INTRODUCTION

Fiber reinforced polymer (FRP) composites, particularly basalt fiber reinforced polymer (BFRP) and glass fiber reinforced polymer (GFRP), have become increasingly popular in civil infrastructure applications due to their excellent mechanical properties, corrosion resistance, and lightweight nature.[1] However, despite their advantages, the long-term durability of FRP materials remains a critical concern, especially in harsh environmental conditions.[2] As infrastructures such as bridges, tunnels, and marine structures are often exposed to alkaline environments, it is crucial to understand how these materials perform under such conditions – an issue that has also been emphasized in the context of intelligent construction and vision-based measurement techniques.[3,4] The degradation of FRP bars in alkaline environments can compromise their mechanical integrity, leading to structural failure, which makes durability prediction a critical component of ensuring a safe and prolonged service life of FRP-reinforced concrete structures.[5]

Over the past decades, considerable research efforts have been devoted to evaluating the durability of FRP bars under various environmental stressors.[6–8] Many

*Corresponding author's e-mail:
LinjieChai@outlook.com (Linjie Chai)

studies have demonstrated that FRP bars exposed to alkaline solutions undergo progressive loss of tensile strength and shear capacity, with the extent of degradation influenced by fiber type, resin system, temperature, and exposure duration.[5,9] Experimental investigations have shown that BFRP bars, although cost-effective and environmentally friendly, often exhibit higher sensitivity to alkaline corrosion compared with GFRP, particularly at elevated temperatures. Moisture absorption has also been recognized as a critical factor accelerating degradation: while the diffusion process initially follows Fick's law, nonlinear absorption behavior emerges as the internal microstructure evolves, indicating that simple linear models are insufficient to capture long-term deterioration. Furthermore, microstructural analyses using techniques such as scanning electron microscopy (SEM) have revealed a sequential degradation pathway, beginning with resin matrix corrosion, followed by fiber–matrix interfacial debonding and eventually fiber dissolution, which collectively lead to void expansion and the formation of corrosion channels.[10,11] These findings underscore the complex and multi-stage nature of FRP deterioration in alkaline environments.

In parallel with experimental research, several modeling approaches have been proposed to predict the long-term performance of FRP bars.[12–14] Classical Fickian diffusion models have been widely employed to describe the relationship between moisture uptake and strength retention. However, such models are limited in their predictive capacity once nonlinear diffusion regimes dominate, particularly when temperature fluctuations and microstructural transformations accelerate deterioration. More advanced models, incorporating multi-phase diffusion processes or coupling chemical reactions with mechanical property degradation, have been developed to address these shortcomings. Nevertheless, existing approaches often fail to fully reconcile experimental observations with predictive outputs, thereby limiting their applicability in practical engineering design and durability assessment.

Therefore, this study aims to bridge the gap in understanding the long-term degradation and service life prediction of BFRP and GFRP bars under alkaline corrosion environments. The primary objective of this study is to explore the deterioration mechanisms of these materials, specifically focusing on the effects of temperature and corrosion time on their mechanical properties. Through accelerated aging tests, this research provides a comprehensive analysis of the tensile strength, shear strength, and moisture absorption characteristics of FRP bars under alkaline conditions. Furthermore, it introduces an improved Fick-based degradation model, which more accurately reflects the nonlinearities observed in the moisture absorption process and predicts the long-term service life of FRP bars.

## 2 EXPERIMENTAL PART

### *2.1 Materials and corrosive environment*

The FRP bars employed in this study were basalt fiber reinforced polymer (BFRP) and glass fiber reinforced polymer (GFRP) bars with an epoxy resin matrix, each having a diameter of 8 mm. According to the requirements of ACI 440.3R-04, the measured tensile strength of the BFRP bars was 1315.4 MPa, while that of the GFRP bars was 1085.7 MPa.[15] The alkaline solution was prepared by mixing 120 g of $Ca(OH)_2$, 1 g of NaOH, 4.5 g of KOH, and 1 L of distilled water. The BFRP and GFRP bars were immersed in alkaline solutions at 20 °C and 40 °C for accelerated aging tests, as illustrated in **Figure 1**.

In practical engineering applications, both ends of the bars are typically anchored, and corrosion solutions permeate radially, which more closely simulates actual service conditions. Therefore, the ends of each specimen prepared for the interlaminar shear strength test were sealed with epoxy adhesive. After the epoxy was fully cured, the specimens were placed in corrosion boxes filled with alkaline solution, which were then immersed in water baths maintained at the designated temperatures. At the end of the predetermined exposure periods, the specimens were removed, dried, and subsequently tested.

This study focused on accelerated degradation of BFRP and GFRP bars under alkaline environments, and the experimental design is summarized in **Table 1**.

**Table 1:** FRP corrosion tests

| Specimen ID | Type | Temperature (°C) | Exposure duration (days) | | | |
|---|---|---|---|---|---|---|
| BFRP-40 | BFRP | 40 | 0 | 30 | 60 | 90 |
| BFRP-60 | BFRP | 60 | 0 | 30 | 60 | 90 |
| GFRP-40 | GFRP | 40 | 0 | 30 | 60 | 90 |
| GFRP-60 | GFRP | 60 | 0 | 30 | 60 | 90 |

### *2.2 Test methods*

The tensile performance test was conducted using a universal testing machine under displacement control

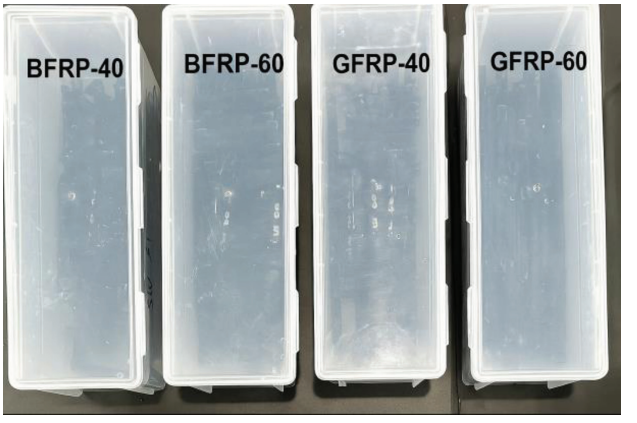


**Figure 1:** Immersion of FRP specimens in alkaline environment

with a loading rate of 2 mm/min. The applied load was recorded by the built-in load cell of the testing machine, while deformation was measured by an extensometer with a gauge length of 100 mm. The tensile strength was calculated according to Equation (1).

The interlaminar shear strength test was also carried out on the universal testing machine under displacement control at a loading rate of 1.5 mm/min, and the interlaminar shear strength was determined using Equation (2).

$$f_u = \frac{F_u}{A} \tag{1}$$

$$\tau_{max} = \frac{V}{3I_z}\left(\frac{d}{2}\right)^2 = \frac{4}{3}\frac{V}{A} = 0.849\frac{F}{D^2} \tag{2}$$

Here, $f_u$ is the tensile strength (MPa), $F_u$ is the maximum tensile load (kN), $A$ is the cross-sectional area (mm$^2$), and $\tau_{max}$ is the maximum transverse shear strength (MPa).

## 3 RESULTS AND ANALYSIS

### *3.1 Surface characteristics*

**Figure 2** shows the surface characteristics of BFRP bars after exposure to alkaline corrosion for different durations. As illustrated, compared with unaged BFRP bars, the surface gloss decreased after 30 days of exposure. After 60 days, a small amount of alkaline crystalline deposits appeared on the bar surface, accompanied by the formation of pores. The resin layer on the outer surface of the BFRP bars exhibited a lighter color, and the amount of crystalline deposits increased significantly. After 90 days of corrosion, cracks developed on the bar surface, the outer resin exhibited clear aging phenomena, and the degree of corrosion intensified.

**Figure 3** presents the surface morphology of GFRP bars under varying corrosion durations. Prior to immersion, the GFRP bar surface appeared relatively rough and lacked gloss. After 30 days of corrosion, alkaline crystalline deposits adhered to the bar surface. At 60 days, the amount of crystalline deposits increased, and the resin between ribs gradually darkened in color. After 90 days, parts of the fibers and resin on the GFRP bar surface turned black, showing signs of swelling and micro-cracking.

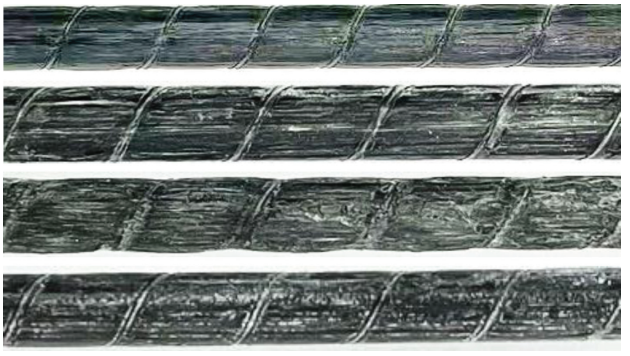

**Figure 2:** Surface characteristics of BFRP bars under alkaline corrosion: a) BFRP-40-0 day, b) BFRP-40-30 days, c) BFRP-40-60 days, d) BFRP-40-90 days

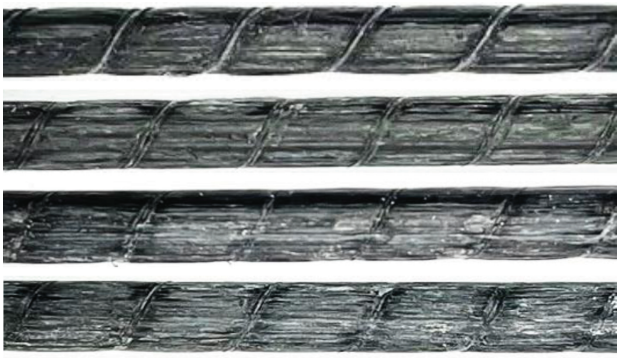

**Figure 3:** Surface characteristics of GFRP bars under alkaline corrosion: a) GFRP-40-0 day, b) GFRP-40-30 days, c) GFRP-40-60 days, d) GFRP-40-90 days

### *3.2 Effect on tensile strength retention*

Tensile strength retention ($R$) serves as the primary metric for evaluating durability. It is defined as the percentage of residual mechanical strength remaining after exposure to the corrosive environment compared to the initial unaged strength. The calculation is expressed as Equation (3).

$$R = \frac{f_t}{f_0} \times 100\% \tag{3}$$

Here, $f_t$ represents the residual strength after exposure time $t$, and $f_0$ represents the initial mechanical strength. The evolution of tensile performance of GFRP and BFRP bars under alkaline corrosion is discussed below.

**Figure 4** illustrates the tensile strength degradation of both GFRP and BFRP bars at 40 °C and 60 °C. At 40 °C, GFRP bars retained 60.6 % of their strength after 90 days, showing a relatively uniform decline. In contrast, BFRP bars degraded rapidly, plummeting to 55.0 % within the first 30 days and ending at 29.0 %. Elevated temperatures (60 °C) exacerbated this trend, with the GFRP and BFRP retention dropping to 36.5 % and 22.3%, respectively. For both materials, the steepest loss occurred in the first month.

At 60 °C, both GFRP and BFRP bars exhibited substantial reductions in tensile strength retention. After 90 days, the tensile strength retention of GFRP bars was 36.5 %, while that of BFRP bars was as low as 22.3 %. For both types of bars, the most pronounced decline occurred within the first 30 days, after which the degradation rate slowed down. Comparisons clearly indicate that the rate of degradation in alkaline solutions at 60 °C was significantly higher than that at 40 °C.

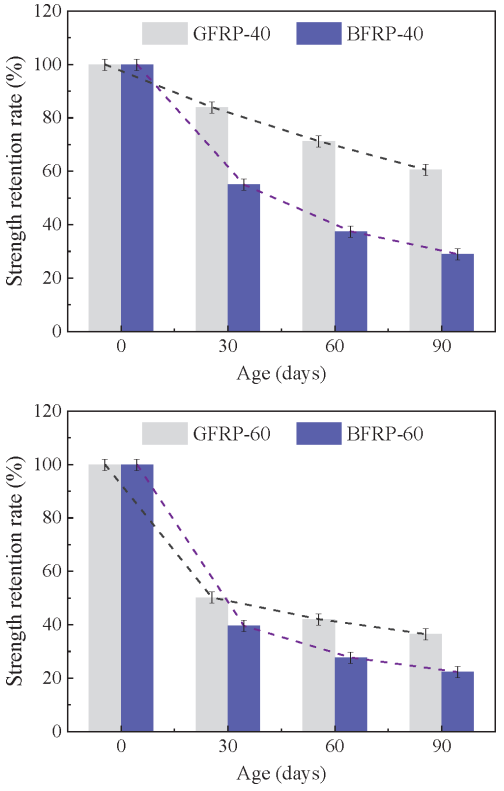


**Figure 4:** Tensile strength degradation of GFRP and BFRP bars under different corrosion environments: a) 40 °C alkaline environment, b) 60 °C alkaline environment

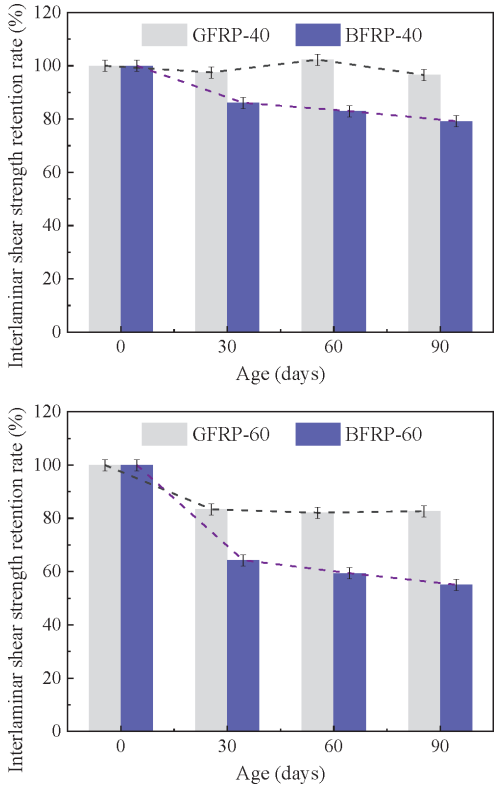


**Figure 5:** Interlaminar shear strength degradation of GFRP and BFRP bars under different corrosion environments: a) 40 °C alkaline environment, b) 60 °C alkaline environment

### *3.3 Effect on interlaminar shear strength*

**Figure 5** displays the interlaminar shear strength retention, revealing that GFRP bars exhibited relatively minor fluctuations at 40 °C, with the overall values remaining close to the unaged condition. Interestingly, after 60 days, the strength retention (100.9 %) slightly increased, which may be attributed to post-curing of the resin and the penetration of water molecules into the bar, alleviating the aggregation of polypropylene (PP) molecules caused by manufacturing imperfections, thereby enhancing strength. In the early stages, the interlaminar shear strength retention of GFRP bars under alkaline corrosion at 40 °C remained stable or even slightly higher than that in pure water environments. This phenomenon may be explained by short-term interfacial strengthening effects arising from humidity and electrochemical interactions in the alkaline medium, such as ion exchange, mild moisture absorption, and charge balance. However, over longer durations, strength degradation inevitably occurred.

In contrast, the interlaminar shear strength of BFRP bars gradually decreased under alkaline corrosion at 40 °C, reaching 79.2 % after 90 days. At 60 °C, the decline was precipitous: retention dropped to 64.3 % in just 30 days and tapered to 55.1 % by the end of the test. Overall, GFRP bars demonstrated superior resistance to alkaline corrosion compared with BFRP bars, while the strength degradation of BFRP bars was more pronounced with increasing temperature.

### *3.4 Effect on moisture absorption*

**Figure 6** depicts the time-dependent moisture absorption behavior of GFRP and BFRP bars. With increasing exposure time, the absorption rate continued to rise but gradually approached a plateau, reflecting a nonlinear growth pattern. This indicates that moisture uptake was relatively rapid at the initial stage, but as internal voids became progressively saturated, the absorption rate slowed down, although the overall accumulation remained positive. This behavior is consistent with Fick's second law of diffusion, which states that diffusion rate depends on the concentration gradient and diffusion coefficient. As water accumulated within the material, the driving force for diffusion weakened, leading to a reduced absorption rate.

Compared with 40 °C, the bars exhibited higher moisture absorption in the 60 °C alkaline environment, which is likely related to microstructural changes induced by elevated temperature. At 60 °C, the molecular motion of the material intensified, increasing porosity and facilitating easier diffusion of water molecules into the internal structure.

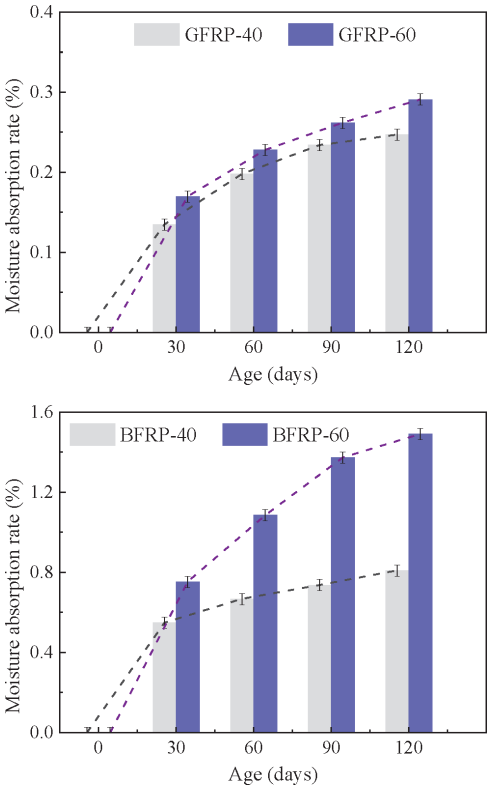


**Figure 6:** Moisture absorption of GFRP and BFRP bars under different corrosion environments: a) GFRP bars, b) BFRP bars

## 4 CORROSION MECHANISM ANALYSIS

### *4.1 SEM microstructural analysis*

As shown in **Figures 7a–7c**, the cross-sections of GFRP bars exposed to alkaline corrosion at 40 °C exhibited increasing microstructural disorder with longer exposure durations. Specifically, fiber alignment became distorted, and their distribution became uneven. A new corrosion feature also appeared: fiber bundles exhibited both agglomeration and dispersion. This phenomenon can be attributed to enhanced penetration of the alkaline solution with extended exposure, which induced swelling within the bar. Consequently, the initially compact arrangement of fiber bundles became locally loosened and separated, while the fiber bundles near the core region remained relatively dense. Such disruption and localized damage to the fiber-bundle structure inevitably weakened the overall mechanical performance of the material.

As observed in **Figures 7d–7f**, the cross-sections of BFRP bars under the same conditions exhibited more severe degradation. Corrosion channels developed along the edges of the bars, which accelerated the diffusion and deep penetration of the alkaline solution. In **Figure 7d**, multiple large voids are present within the cross-section. These enlarged voids not only served as deposition sites for corrosion products but also weakened the inter-fiber support mechanism, resulting in a reduction in the long-term tensile performance of the bars. In **Figure 7f**, the edges of the bars appear visibly loosened. This phenomenon of edge fiber loosening significantly contributes to the overall mechanical degradation. As the outer fiber layers detach from the matrix and loosen, they lose the ability to transfer stress efficiently, effectively reducing the load-bearing cross-sectional area of the bar. Consequently, the applied load is concentrated on the remaining core fibers, leading to premature failure. Furthermore, this loosened peripheral structure creates a porous pathway that facilitates the rapid ingress of corrosive ions into the bar's interior, thereby accelerating the deterioration of the initially intact core. Collectively, **Figures 7d–7f** indicate that, with increasing exposure duration, the synergistic effects of alkaline corrosion led to progressive edge fiber loosening, void expansion, and the formation of corrosion channels. These microstructural changes further compromised the long-term mechanical properties of the bars, which was consistent with the previously observed degradation trends in tensile strength and interlaminar shear strength.

### *4.2 Corrosion mechanism analysis*

BFRP and GFRP bars are primarily composed of epoxy resin matrices and reinforcing fibers. Both materials share similar skeletal structures and chemical compositions; consequently, they undergo comparable physical processes and chemical reactions under alkaline environments. The overall corrosion process can be categorized into three stages: resin matrix corrosion, fiber corrosion, and interfacial corrosion.

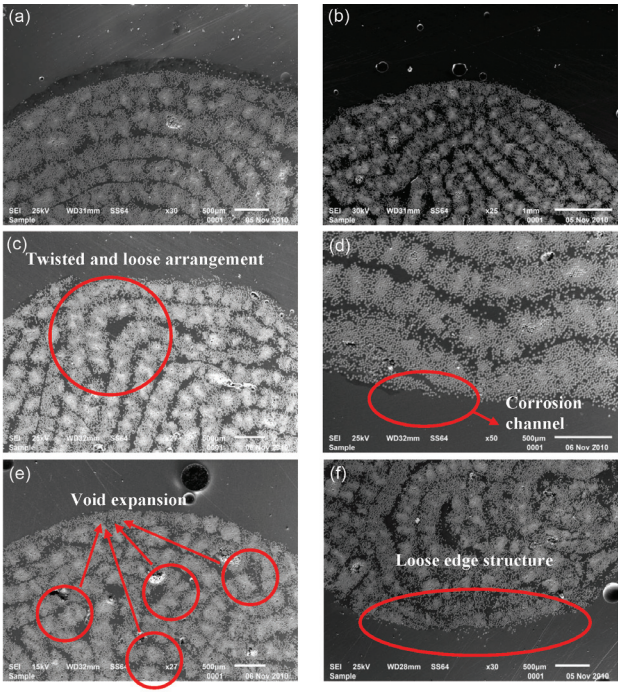


**Figure 7:** SEM observations of cross-sections: a) GFRP-40-30 days, b) GFRP-40-60 days, c) GFRP-40-90days, d) BFRP-40-30 days, e) BFRP-40-60 days, f) BFRP-40-90 days

The preceding analysis indicates that 30 days of exposure represents a critical inflection point in the mechanical property degradation of FRP bars. During the first 30 days, corrosion primarily affects the resin matrix. In the early stage, alkaline solution penetrates into the interior of the bars through diffusion and permeation, resulting in a substantial hydrostatic pressure gradient between the interior and exterior. This induces localized stress at the fiber–resin interface. Moreover, permeation contributes to the initiation of microcracks on the bar surface, which further accelerates water uptake by the resin matrix.

As exposure continues, increasing amounts of water molecules and $OH^-$ ions infiltrate the resin, causing swelling and increasing resin plasticity. Simultaneously, hydrolysis reactions occur between water molecules and the resin, as expressed with Equation (4). This hydrolysis leads to debonding of the resin, thereby reducing the tensile strength and elastic modulus of the FRP bars, although the magnitude of reduction during this stage remains relatively modest.

$$RCOO - R' + H2O \rightarrow RCOO - H + R'OH \quad (4)$$

Beyond 30 days of exposure, interfacial and fiber corrosion become dominant. Hydrolysis of the resin generates additional $OH^-$ ions, which elevate the alkalinity of the solution. Water molecules and $OH^-$ ions penetrate the fiber–resin interface, causing debonding, while also directly attacking the fibers through etching reactions.

This further accelerates fiber hydrolysis, as represented in Equations (5) and (6). Within the fibers, Si–O bonds react with $OH^-$ ions from the solution, leading to bond cleavage and the breakdown of the $SiO_2$ network structure. This deterioration mechanism degrades both basalt and glass fibers, ultimately resulting in significant reductions in tensile strength and elastic modulus of FRP bars. From the SEM micrographs, it is evident that tensile strength degradation is primarily governed by interfacial debonding and fiber damage, while the reduction in elastic modulus is more strongly influenced by the type of fiber and the extent of its degradation.

$$Si - O - Si + OH^- \rightarrow Si - OH + Si - O^- \quad (5)$$

$$Si - O^- + H2O \rightarrow Si - OH + OH^- \quad (6)$$

## 5 SERVICE LIFE PREDICTION OF CORROSION RESISTANCE

### *5.1 Improved Fick degradation model*

The Fick degradation model is derived from Fick's second law of diffusion, which describes the transport of ions within the bar material. Through a series of reasonable assumptions, this law has been extended into a predictive model for the service life of FRP bars. The internal ion diffusion state of the bars is reflected in the moisture absorption curve as a function of time. Prior to reaching the critical saturation point, the absorption process is defined as the "Fick stage," during which the moisture uptake strictly follows the description of Fick's second law. However, once the absorption exhibits a nonlinear acceleration, the bar enters the "non-Fick stage," when the Fick degradation model loses predictive validity.

The primary limitation of traditional Fickian models is their reliance on a constant diffusion coefficient derived solely from the initial linear absorption phase. This approach often leads to significant prediction errors when the material exhibits non-Fickian behavior or when moisture uptake slows down in the nonlinear stage. The "improved Fick degradation model" proposed in this study addresses this shortcoming by introducing a time-dependent concentration parameter ($C$) and adjusting the calculation of the diffusion coefficient ($D$) to reflect the evolving internal concentration gradient. Unlike the traditional static assumption, this improved approach dynamically correlates the moisture content with the effective load-bearing area, thereby providing a more accurate prediction of strength retention over long-term exposure.

When applying the Fick model, it is assumed that the portion of the bar penetrated by the corrosive solution

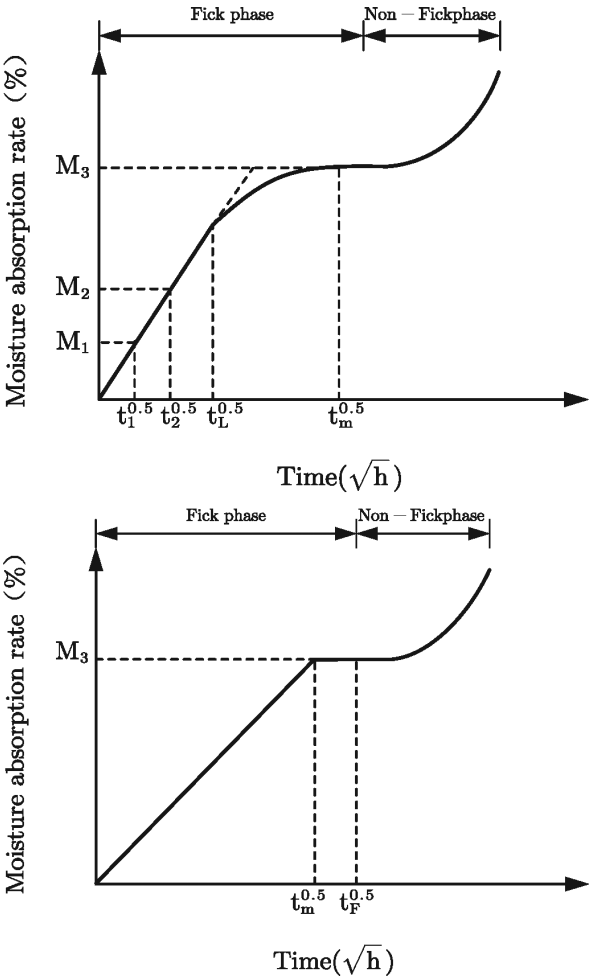


**Figure 8:** Moisture absorption versus time before and after model modification: a) before modification[16], b) after modification[12]

has completely failed and lost its load-carrying capacity, while the unpenetrated region remains intact with full strength and material properties. A key parameter in the Fick diffusion model is the diffusion coefficient, $D$, which is typically determined experimentally by analyzing the moisture absorption–time curve, as illustrated in **Figure 8**. Within the Fick stage, the absorption curve can be divided into a linear stage and a nonlinear stage. These two regimes correspond to different computational models for $D$: namely, the single-stage model and the two-stage model.

In the single-stage model, the diffusion coefficient $D$ of FRP bars is calculated according to Equation (7), when $t^{0.5} < t_L^{0.5}$.

$$D = \frac{\pi r_0^2}{16}\left(\frac{M_2 - M_1}{M_m}\right)^2\left(\frac{1}{\sqrt{t_2} - \sqrt{t_1}}\right)^2 \tag{7}$$

Here, $M_m$ is the maximum moisture content at saturation; $M_1$ and $M_2$ are the moisture contents corresponding to times $t_1^{0.5}$ and $t_2^{0.5}$, respectively. The above equation can be reformulated as Equation (8):

$$D = \frac{\pi r_0^2 k^2}{16 M_m^2} \tag{8}$$

Where $k = (M_2 - M_1)/(\sqrt{t_2} - \sqrt{t_1})$ represents the slope of the linear stage in **Figure 8**. In the improved model, the calculation of $D$ still follows Equation (9), but here $k$ is no longer derived from the linear stage in Figure 8a, but rather from the linear stage illustrated in Figure 8b. Thus, Equation (9) is obtained:

$$k = \frac{M_m}{t_m^{0.5}} \tag{9}$$

Substituting Equation (9) into Equation (8) yields Equation (10):

$$D = \frac{\pi r_0^2}{16 t_m} \tag{10}$$

Since $\sqrt{t}/\sqrt{t_m} = M/M_m$, the above can be further simplified to Equation (11):

$$P_p = P_0\left(1 - \frac{\sqrt{t}}{\sqrt{t_m}}\sqrt{\frac{\pi C}{8}}\right)^2 \tag{11}$$

Equation (11) represents the improved Fick degradation model. Compared with the original formulation, the improved equation no longer includes the radius $r$. This omission does not imply that bar diameter has no influence on corrosion, but rather that this effect is captured indirectly through other parameters. Letting $\lambda$ denote the strength retention ratio, Equation (12) can be derived:

$$\lambda = \left(1 - \frac{M}{M_m}\sqrt{\frac{\pi C}{8}}\right)^2 \tag{12}$$

In this formulation, $M$ and $M_m$ denote the actual and saturated moisture contents, respectively, as obtained from absorption curves. The parameter $C$ varies with the corrosion time and reflects the ratio of internal ion concentration to solution concentration. Based on the experimental data presented in Section 3, the evolution of $C$ over time is determined. Equation (12) indicates that when saturation is reached ($M = M_m$), the strength retention ratio $\lambda$ is governed by $C$. If $C$ remains constant, $\lambda$ does not change, which contradicts experimental results. Thus, the variation of $C$ drives the corrosion process. The model is valid during the Fick stage (i.e., prior to cracking and after saturation), where solution concentration increases, corrosion depth expands, and strength retention decreases. Beyond this stage, the model is no longer applicable.

The specific procedure for predicting the service life of FRP bars in solution using the Fick degradation model is as follows:

1) Determine the threshold of saturated moisture content. Based on the moisture absorption–time curve and the proposed linear model, identify the maximum moisture content $M_m$.
2) Calculate the moisture content at specific time points. Using linear regression of the absorption curve, compute the moisture content at various corrosion ages.
3) Back-calculate the evolution of parameter $C$. With known strength retention ratios $\lambda$ from Section 3 and the corresponding values of $M$ and $M_m$, use Equation (11) to inversely derive the time-dependent evolution of $C$.
4) Fit the evolution of parameter $C$. Based on the principle of Fick's second law, fit the temporal evolution of $C$ with an exponential function.
5) Predict strength retention. Using the fitted function of $C$, the saturated moisture content $M_m$, and the moisture content $M$ at each time point, apply Equation (12) to predict the strength retention ratio $\lambda$ at any given time during the Fick stage, thereby enabling comprehensive service life prediction of FRP bars in solution environments.

### *5.2 Service life prediction of FRP bars*

It is assumed that within the maximum exposure duration considered (90 days), the bars did not reach the saturated moisture state and thus remained in the Fick diffusion stage. Based on the improved Fick degradation model, predictions of the service life of the bars were conducted.

The linear portions of the moisture absorption–time curves for the different corrosion environments were fitted, and the results are presented in **Figure 9**.

The saturated moisture contents of the different specimens were determined from the absorption experiments, as summarized in **Table 2**. It was found that the saturated moisture content $M_m$ of the GFRP-40 specimen increased

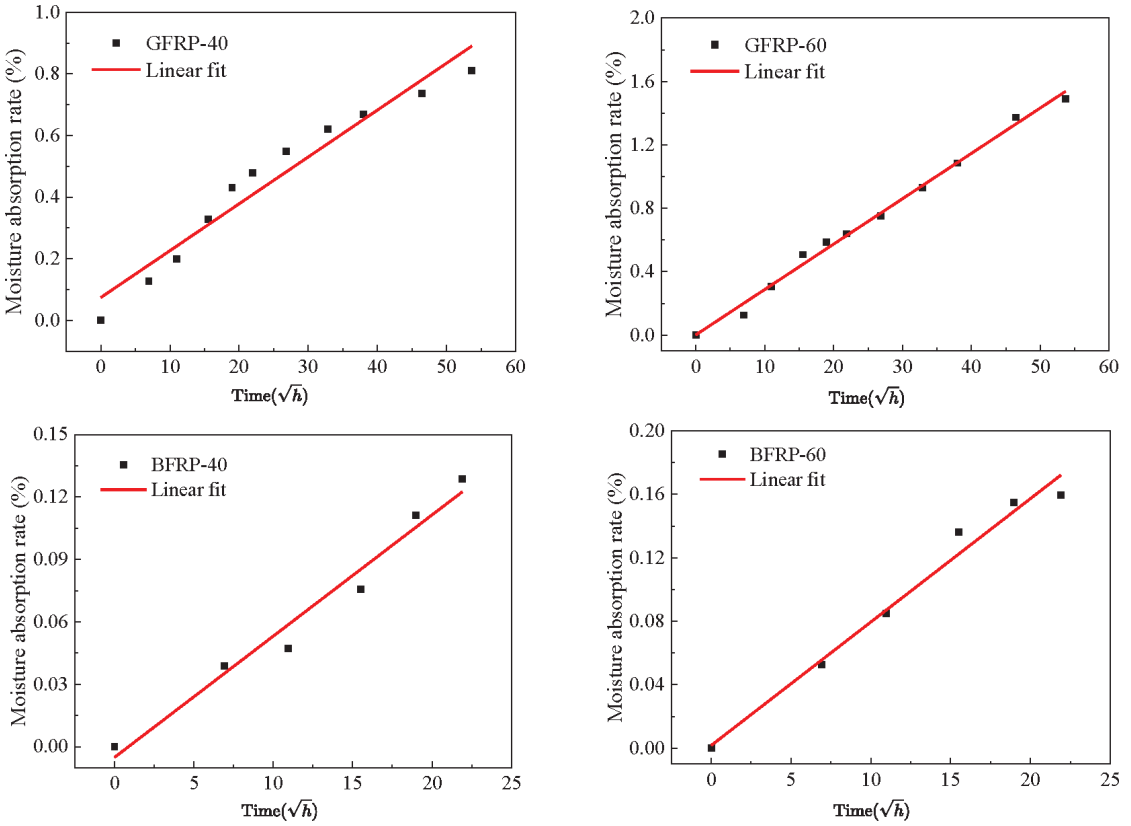


**Figure 9:** Linear fitting of moisture absorption for GFRP and BFRP bars under different corrosion environments: a) GFRP in 40 °C alkaline environment, b) GFRP in 60 °C alkaline environment, c) BFRP in 40 °C alkaline environment, d) BFRP in 60 °C alkaline environment

**Table 2:** Parameters of the Fick degradation model

| Specimen ID | Intercept $a$ | Slope $b$ | Age/$\sqrt{h}$ | $M$ | $M_m$ | Experimental strength retention (%) | $C$ |
|---|---|---|---|---|---|---|---|
| GFRP-40 | 0.0743 | 0.0152 | 25.9 | 0.468 | 0.810 | 86.15 | 0.039330 |
| | | | 36.7 | 0.632 | | 82.97 | 0.033269 |
| | | | 44.9 | 0.757 | | 79.19 | 0.035384 |
| GFRP-60 | 0.0017 | 0.0286 | 25.9 | 0.744 | 1.491 | 64.35 | 0.400418 |
| | | | 36.7 | 1.051 | | 59.42 | 0.268972 |
| | | | 44.9 | 1.287 | | 55.13 | 0.226554 |
| BFRP-40 | 0.0051 | 0.0058 | 25.9 | 0.146 | 0.247 | 97.52 | 0.001141 |
| | | | 36.7 | 0.208 | | 97.72 | 0.000471 |
| | | | 44.9 | 0.256 | | 82.13 | 0.020828 |
| BFRP-60 | 0.0018 | 0.0078 | 25.9 | 0.203 | 0.291 | 83.44 | 0.038971 |
| | | | 36.7 | 0.287 | | 82.13 | 0.022980 |
| | | | 44.9 | 0.351 | | 82.68 | 0.014368 |

to 0.810, indicating enhanced moisture absorption capacity with elevated temperature. For the GFRP-60 specimen, $M_m$ reached as high as 1.491, significantly exceeding the former. A similar trend was observed for the BFRP series: the $M_m$ of BFRP-40 was 0.247, while that of BFRP-60 further increased to 0.291. These results demonstrate that, for both GFRP and BFRP bars, higher temperatures led to increased moisture absorption.

The Fick degradation model addresses cases where corrosive ions of a certain concentration diffuse into the interior of the bars and induce degradation. Although water molecules may cause swelling and degradation, pure water itself does not possess concentration gradients. Therefore, in a pure water environment, diffusion is not further driven by concentration differences, and the improved Fick degradation model cannot be applied to predict service life in such conditions.

The analysis focuses on the GFRP-40 and BFRP-40 specimens, considering the applicability limits of the Fick diffusion model. Fick's law is fundamentally suited for describing diffusion processes under constant temperature. In environments with temperature fluctuations, diffusion rates are strongly influenced, and direct appli-

cation of Fick's model may yield insufficiently accurate or even erroneous results.

The experimentally determined values of parameter $C$ under different environments were fitted using exponential functions, as illustrated in **Figure 10**. The curves demonstrate good agreement and high fitting accuracy, confirming that an exponential function is appropriate to describe the relationship between $C$ and environmental conditions with high predictive reliability.

From the fitting results, the relationship between relative ion concentration $C$ and time $t_{0.5}$ can be expressed as shown in **Table 3**.

Using the above equation, the values of parameter $C$ at different exposure durations can be calculated, and thus the corresponding strength retention ratios of the bars can be predicted. The maximum value of parameter $C$ is limited to 1, since the internal ion concentration of the bar cannot exceed that of the external solution. By analyzing the variation of $C$ under different corrosion conditions, the durability and mechanical degradation of FRP bars can be indirectly assessed. The predicted strength retention ratios at different corrosion ages are listed in **Table 4**.

Based on the strength retention data from **Table 4**, the degradation trends of interlaminar shear strength with corrosion time were plotted, as shown in **Figure 11**. The figure includes experimental data up to 84 days and compares them with the predicted values obtained using

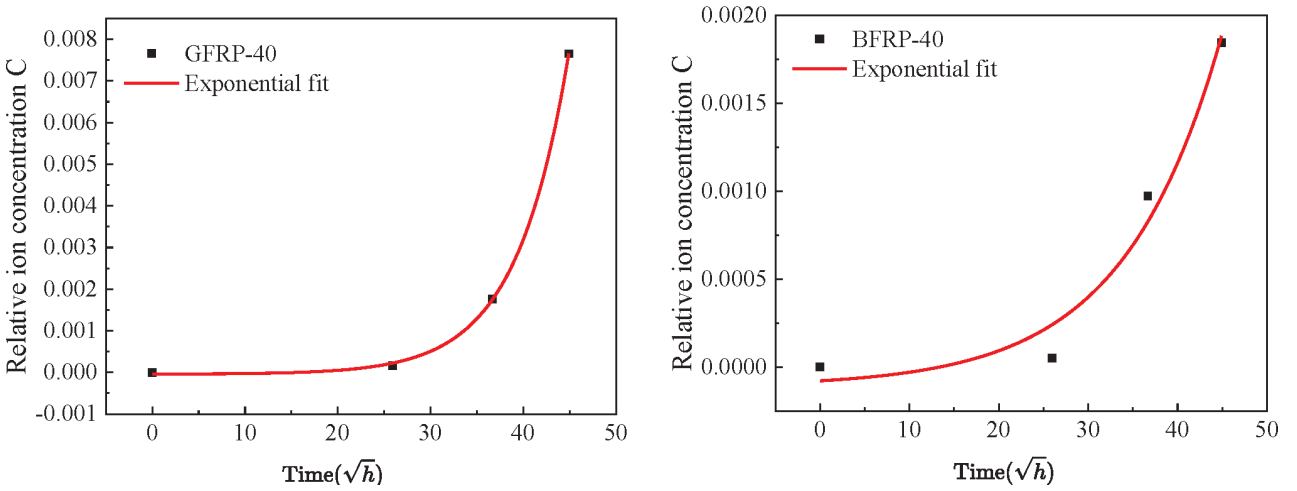


**Figure 10:** Exponential fitting of relative ion concentration $C$: a) GFRP-40 specimen, b) BFRP-40 specimen

**Table 3:** Parameters of the fitted relationship between $C$ and time $\sqrt{h}$

| Specimen ID | Equation | $A_1$ | $t_1$ | $y_0$ |
|---|---|---|---|---|
| GFRP-40 | | 2.7158E-6 | -5.64751 | 4.33503E-5 |
| BFRP-40 | | 3.26939E-5 | -10.92394 | 1.11265E-4 |

**Table 4:** Predicted strength retention ratios

| Specimen ID | Age (days) | $C$ | $M$ | $M_m$ | Strength retention (%) |
|---|---|---|---|---|---|
| GFRP-40 | 7 | 0.000000 | 0.131 | 0.622 | 100.00 |
| | 10 | 0.000000 | 0.164 | | 100.00 |
| | 20 | 0.000088 | 0.245 | | 99.54 |
| | 40 | 0.000612 | 0.361 | | 98.21 |
| | 60 | 0.002206 | 0.450 | | 95.78 |
| | 80 | 0.006317 | 0.525 | | 91.76 |
| | 100 | 0.015850 | 0.591 | | 85.56 |
| | 120 | 0.036331 | 0.620 | | 77.59 |
| BFRP-40 | 7 | 0.000000 | 0.049 | 0.187 | 100.00 |
| | 10 | 0.000000 | 0.058 | | 100.00 |
| | 20 | 0.000132 | 0.080 | | 99.39 |
| | 40 | 0.000446 | 0.112 | | 98.42 |
| | 60 | 0.000943 | 0.136 | | 97.22 |
| | 80 | 0.001694 | 0.157 | | 95.73 |
| | 100 | 0.002787 | 0.175 | | 93.92 |
| | 120 | 0.004335 | 0.190 | | 91.80 |

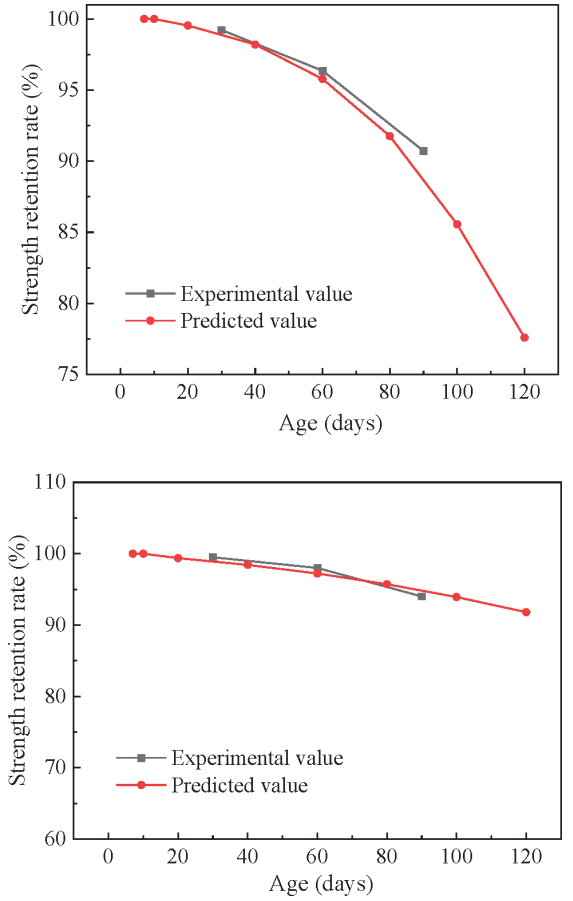


**Figure 11:** Predicted strength retention under different corrosion conditions: a) GFRP-40 specimen, b) BFRP-40 specimen

the Fick degradation model in order to evaluate the accuracy of the model in predicting service life.

As shown in **Figure 11**, the predicted strength retention curves exhibit strong agreement with the experimental results, displaying a high degree of similarity. This indicates that, within the studied period of 120 days, the Fick degradation model provides accurate predictions of the short-term degradation trend of interlaminar shear strength in FRP bars.

## 6 CONCLUSIONS

This study systematically investigated the long-term degradation and service life of basalt fiber–reinforced polymer (BFRP) and glass fiber–reinforced polymer (GFRP) bars in alkaline environments. Accelerated aging tests were conducted at elevated temperatures, and changes in tensile strength, interlaminar shear strength, and moisture absorption were analyzed. Microstructural damage was examined using SEM, and an improved Fick-based model was developed to predict long-term performance. The findings support a durable and safe use of FRP bars in civil infrastructure.

While both materials experienced degradation, GFRP bars demonstrated superior alkaline resistance compared to BFRP bars. BFRP bars exhibited rapid strength loss, particularly at elevated temperatures (60 °C), indicating a higher sensitivity to alkaline attack.

Moisture uptake initially followed Fickian diffusion but transitioned into nonlinear regimes over time. Elevated temperatures accelerated this process, facilitating faster diffusion and microstructural damage that exacerbated mechanical deterioration.

Microstructural analysis revealed a degradation sequence initiating with matrix corrosion, progressing to interfacial debonding and fiber etching. The formation of corrosion channels, void expansion, and edge fiber loosening were identified as the primary drivers of tensile strength and modulus reduction.

The improved Fick-based degradation model, which accounts for time-dependent changes in diffusion, accurately predicted strength retention. The model showed strong agreement with experimental data, validating its applicability for durability assessment in engineering practice.

This study was limited to accelerated aging at constant temperatures (40 °C and 60 °C) over 90 days. Future research should validate the model under more realistic conditions – including temperature fluctuations and mechanical loading – and extend the observation period to refine service life predictions.

## Acknowledgment

The work described in this paper was supported by the Science and Technology Project of State Grid Hebei Electric Power Co., Ltd., entitled Research on Prefabricated Joints for Pile Foundations of Transmission Line Structures (KJ2020 - 035).

## 7 REFERENCES

[1] J. Zhao, H. J. Pan, Z. Wang, J. X. Duan, P. Wang, F. Wang, Christopher K. Y. Leung, Bond durability of BFRP and GFRP bars in sulphoaluminate cement concrete under water immersion environment, Constr. Build. Mater., 432 (**2024**), 136521, doi:10.1016/j.conbuildmat.2024.136521

[2] Y. X, Zhang, K. Y. Hu, J. J. Zeng, W. Hou, Long-term bond performance of fiber-reinforced polymer (FRP) bars to concrete in marine environments: a comprehensive review, Arch. Civ. Mech. Eng., 25 (**2025**), 118, doi:10.1007/s43452-025-01162-1

[3] Y. F. Gu, J. Wu, C. Y. Liu, Error analysis and accuracy evaluation method for coordinate measurement in transformed coordinate system, Measurement, 242 (**2025**), 115860, doi:10.1016/j.measurement.2024.115860

[4] C. Y. Liu, J. Wu, Y. F. Gu, L. Q. Xie, G. Wu, Binocular vision-based guidance for robotic assembly of prefabricated components, Autom. Constr., 172 (**2025**), 106065, doi:10.1016/j.autcon.2025.106065

[5] M. A. Rifai, H. E. Hassan, T. E. Maaddawy, F. Abed, Durability of basalt FRP reinforcing bars in alkaline solution and moist concrete environments, Constr. Build. Mater., 243 (**2020**), 118258, doi:10.1016/j.conbuildmat.2020.118258

[6] J. D. Ortiz, S. S. Khedmatgozar, P. Malla, A. Nanni, A. Mehrabi, FRP-reinforced/strengthened concrete: State-of-the-art review on durability and mechanical effects, Materials, 16 (**2023**), 1990, doi:10.3390/ma16051990

[7] X. L. Hu, J. Z. Xiao, K. J. Zhang, Q. T. Zhang, The state-of-the-art study on durability of FRP reinforced concrete with seawater and sea sand, Build. Eng., 51 (**2022**), 104294, doi:10.1016/j.jobe.2022.104294

[8] J. L. Li, Z. H. Mai, J. H. Xie, Z. Y. Lu, Durability of components of FRP-concrete bonded reinforcement systems exposed to chloride environments, Compos. Struct., 279 (**2022**), 114697, doi:10.1016/j.compstruct.2021.114697

[9] J. H. Xie, Y. C. Li, Z. Y. Lu, Z. H. Fan, J. L. Li, S. X. Li, Effects of immersion in water, alkaline solution, and seawater on the shear performance of basalt FRP bars in seawater–sea sand concrete, Compos. Constr., 26 (**2022**), 04021071, doi:10.1061/(ASCE)CC.1943-5614.0001184

[10] P. Wang, L. Y. K. Ke, Z. K. Wang, J. Zhao, W. W. Li, C. K. Y. Leung, Effects of alkaline concentration and saline contents on degradation of tensile properties, microstructure and chemical characterization of glass fiber reinforced polymer (GFRP) rebars, Build. Eng., 69 (**2023**), 106222, doi:10.1016/j.jobe.2023.106222

[11] Y. Fang, T. Hu, L. J. Qiao, F. Yu, L. Zhang, H. R. Sun, C. Li, Alkali-activated metakaolin-blast furnace slag blends as an alternative inorganic adhesive for FRP-based structural rehabilitation, Build. Eng., 103 (**2025**), 112163, doi:10.1016/j.jobe.2025.112163

[12] A. Y. Xu, Y. X. Du, A. F. Guo, W. P. Pan, D. J. Zhu, Durability and long-term life prediction of hybrid FRP bars embedded in SSC under seawater environment, Compos. Part B-Eng., 292 (**2025**), 112094, doi:10.1016/j.compositesb.2024.112094

[13] J. B. Sun, J. F. Zhang, Y. F. Gu, Y. M. Huang, Y. T. Sun, G. W. Ma, Prediction of permeability and unconfined compressive strength of pervious concrete using evolved support vector regression, Constr. Build. Mater., 207 (**2019**), 440–449, doi:10.1016/j.conbuildmat.2019.02.117

[14] C. Machello, M. Rahmati, M. Bazli, A. Rajabipour, M. Arashpour, R. Hassanli, M. Shakiba, Machine learning-based prediction of bond performance of FRP composite bars in concrete for marine composite structures, Compos. Struct., 370 (**2025**), 1–19, doi:10.1016/j.compstruct.2025.119401

[15] ACI Committee 440, Guide test methods for fiber-reinforced polymers (FRPs) for reinforcing or strengthening concrete structures, American Concrete Institute, 2025